

Research Article

## Na<sup>+</sup> Mobility in PEO-Based Composite Solid-State Electrolytes by NMR

Fariba Moradipour <sup>1,†</sup>, Andreas Markert <sup>1,†</sup>, Thomas Rudszuck <sup>1</sup>, Niklas Röttgen <sup>2</sup>, Gerald Dück <sup>3</sup>, Martin Finsterbusch <sup>3</sup>, Felix Gerbig <sup>1</sup>, Hermann Nirschl <sup>1</sup>, Gisela Guthausen <sup>1,4,\*</sup>

1. Institute of Mechanical Process Engineering and Mechanics, Karlsruhe Institute of Technology (KIT), Karlsruhe, Germany; E-Mails: [ucnds@student.kit.edu](mailto:ucnds@student.kit.edu); [andreas.markert@kit.edu](mailto:andreas.markert@kit.edu); [thomas.rudszuck@kit.edu](mailto:thomas.rudszuck@kit.edu); [felix.gerbig@kit.edu](mailto:felix.gerbig@kit.edu); [hermann.nirschl@kit.edu](mailto:hermann.nirschl@kit.edu); [gisela.guthausen@kit.edu](mailto:gisela.guthausen@kit.edu)
2. ICT, Fraunhofer Institute for Chemical Technology, Joseph-von-Fraunhofer-Str. 7, 76327 Pfinztal, Germany; E-Mail: [niklas.roettgen@ict.fraunhofer.de](mailto:niklas.roettgen@ict.fraunhofer.de)
3. IEK-1, Forschungszentrum Jülich, 52425 Jülich, Germany; E-Mails: [g.dueck@fz-juelich.de](mailto:g.dueck@fz-juelich.de); [m.finsterbusch@fz-juelich.de](mailto:m.finsterbusch@fz-juelich.de)
4. Engler Bunte Institut, Chair of Water Chemistry and Water Technology, KIT, D-76131 Karlsruhe, Germany

† These authors contributed equally to this work.

\* **Correspondence:** Gisela Guthausen; E-Mail: [gisela.guthausen@kit.edu](mailto:gisela.guthausen@kit.edu)

**Academic Editor:** Vitaly I. Volkov

**Special Issue:** [NMR Techniques for Electrolytes of Batteries](#)

*Journal of Energy and Power Technology*  
2023, volume 5, issue 4  
doi:10.21926/jept.2304032

**Received:** August 04, 2023  
**Accepted:** October 22, 2023  
**Published:** November 02, 2023

### Abstract

Charge transfer and mobility are essential for electrochemical processes in batteries, which need to be understood in detail for optimization, especially in the case of all-solid-state batteries. Wide line NMR is well-known in solid-state NMR and allows the quantification of ion mobility in ordered crystalline and amorphous structures. Temperature-dependent <sup>23</sup>Na-NMR is sensitive to ion mobility via longitudinal relaxation, but also via line analysis and transverse relaxation. As <sup>23</sup>Na is a spin 3/2 nucleus, <sup>23</sup>Na-NMR is also susceptible to electric field gradients caused by their nearest neighbor environment and, therefore, reflects not only



© 2023 by the author. This is an open access article distributed under the conditions of the [Creative Commons by Attribution License](#), which permits unrestricted use, distribution, and reproduction in any medium or format, provided the original work is correctly cited.

the mobility of  $^{23}\text{Na}^+$  but also the molecular dynamics in the neighborhood, which are investigated in this paper. The named NMR methods were explored to study  $^{23}\text{Na}^+$  mobility in the solid electrolytes NaSICON (sodium (Na) Super Ionic CONductor, here  $\text{Na}_{3.4}\text{Zr}_2\text{Si}_{2.4}\text{P}_{0.6}\text{O}_{12}$ ), the salt NaTFSI (sodium bis(trifluoromethyl sulfonyl)imide), as well as in the polymer-based electrolytes PEO-NaSICON, PEO-NaTFSI, and PEO-NaTFSI-NaSICON.

## Keywords

Wideline NMR; transverse relaxation; solid electrolyte; ion mobility; NaSICON; NaTFSI; PEO-composite polymeric electrolytes CPE

## 1. Introduction

Solid electrolytes are a prospective alternative to liquid electrolytes [1] for Lithium (Li) and Sodium (Na) batteries. Degradation phenomena such as leakage or dendrite growth are significantly reduced, which are a constant threat in established battery systems [2]. Therefore, solid electrolytes promise prolonged cycle life [3, 4], which is especially crucial for batteries in stationary energy storage applications. In the past, different types of electrolytes have been studied: Inorganic ceramic electrolytes (ICE), solid polymeric electrolytes (SPE), and composite polymeric electrolytes (CPE). Examples of  $\text{Na}^+$ -conducting ICE are NaSICONs as  $\text{Na}_{3.4}\text{Zr}_2\text{Si}_{2.4}\text{P}_{0.6}\text{O}_{12}$ , while the salts NaTFSI and NaFSI are used in SPE and CPE [5-9]. Ceramic electrolytes feature high ionic conductivity but are brittle. Solid polymeric electrolytes offer good mechanical flexibility and good contacting while suffering from low ionic conductivities, especially at ambient temperature due to the lower ion mobility caused by interactions of  $\text{Na}^+$  with the oxygen in PEO (poly (oxyethylene) or poly (ethylene oxide)). In summary, solid polymer electrolytes contain dissolved salts for  $\text{Na}^+$  conduction, while inorganic ceramic electrolytes possess an intrinsic  $\text{Na}^+$  conductivity.

Composite polymer electrolytes incorporate inorganic salts or ceramics in a polymer host matrix, combining the advantages of both classes of solid electrolytes [6]. Generally, the polymer matrix is solvent-free and contains Na-containing substances, here NaTFSI or the NaSICON  $\text{Na}_{3.4}\text{Zr}_2\text{Si}_{2.4}\text{P}_{0.6}\text{O}_{12}$ . The polycrystalline structure of  $\text{Na}_{3.4}\text{Zr}_2\text{Si}_{2.4}\text{P}_{0.6}\text{O}_{12}$  is a mixture of a rhombohedral and a monoclinic phase [10]. The NaTFSI crystal structure is monoclinic [11]. These prevalent materials are used as active fillers in CPE for SIB (sodium ion battery), as described for example in reference [6]. While NaSICONs as a ceramic will preferentially be distributed as particles in the PEO network, the salt NaTFSI will preferentially be dissolved, leading to direct ionic conductivity. Temperature, i.e., the state of PEO, will influence the ion's mobility in the network [12-16].

An important measure to assess the performance of battery materials is the solid-state diffusion coefficient in the solid electrolytes. A reliable measurement of these diffusion coefficients in battery materials also fosters the parameterization of battery models. Such models are crucial for studying otherwise hardly detectable processes inside a battery at convenient temperatures and are inevitable for the accelerated development of advanced battery systems.

Given the increasing demand for large-scale energy storage, there is a strong interest in replacing the established  $\text{Li}^+$ -ion technology with technologies comprising more abundant materials like Na. The ion sizes of  $\text{Na}^+$  (0.102 nm) compared to  $\text{Li}^+$  (0.076 nm) significantly differ, requiring

investigations of the material properties. Na<sup>+</sup> mobility facilitates the endeavor of finding high-performance solid electrolytes for all-solid Na<sup>+</sup> batteries (AS-SIB). However, reliable values of the solid-state diffusion coefficient, or more generally, the ion's mobility, are hardly available. The spread is large and depends on the measurement technique as well as on data treatment, often based on assumptions (for example, reported coefficients range from 10<sup>-17</sup> m<sup>2</sup>/s [17] to 10<sup>-10</sup> m<sup>2</sup>/s [18] at room temperature for the diffusion coefficient of Li<sup>+</sup> in graphite).

NMR is well known to be a suitable analytical tool to study ion mobility in solids. While the translational mobility in liquids is often studied by pulsed field gradient NMR leading to diffusion coefficients in hindered, restricted and free environments [14, 19-26], mobility in solids is most often addressed by relaxation studies [27-33]. Usually, the maximum of the longitudinal relaxation rate as a function of temperature  $T$ ,  $R_{1, \max}(T)$ , is considered, where the correlation time  $\tau_c$  is known to be equal to the inverse Larmor frequency within the 3D BPP model [30, 34-37]. The activation energy  $\Delta E_a$  of the ion's mobility can then be deduced in the solid.

The relaxation approach is in the focus of the investigations to quantify Na<sup>+</sup> low-frequency fluctuations in the diverse environments of a ceramic, a salt, and the corresponding CPE based on PEO: Line width  $\delta\nu(T)$  and transverse relaxation  $R_2(T)$  are studied instead of  $R_1(T)$  or the spin lock relaxation  $R_{1\rho}(T)$  [38] in a temperature range relevant for battery application. Using a BPP-like model with spectral densities for 2D and 3D hopping for  $R_2(T)$ , including quadrupolar interactions similar to [39], will lead to the activation energy of the ion mobility, assuming that the ions take specific sites in the lattices given by energy minima. The dimensionality of Na<sup>+</sup> hopping in the composites is under discussion [30, 31]. Therefore, both approaches will be applied and compared: 2D hopping needs a different spectral density and is compared to the 3D approach [38, 40]. An effective solid-state Na<sup>+</sup> diffusion coefficient can be calculated within the frame of thermal activation by estimating the distances between the sites along the morphology. This methodology is applied to Na<sup>+</sup> in a NaSICON, specifically Na<sub>3.4</sub>Zr<sub>2</sub>Si<sub>2.4</sub>P<sub>0.6</sub>O<sub>12</sub>, and NaTFSI. The NMR methods allow for the study of the impact of the PEO (poly (ethylene oxide)) network on the ion mobility of ceramics and salt dispersed in PEO.

## 2. Materials and Methods

### 2.1 Materials and Synthesis

In this paper, the Na<sup>+</sup> conductor Na<sub>3.4</sub>Zr<sub>2</sub>Si<sub>2.4</sub>P<sub>0.6</sub>O<sub>12</sub> (NaSICON) was investigated as powder and as a dense pellet. It was synthesized employing the solution-assisted solid-state reaction (SA-SSR) technique, as outlined in [41]. Stoichiometric amounts of NaNO<sub>3</sub> (Merck, ACS grade), ZrO(NO<sub>3</sub>)<sub>2</sub> × H<sub>2</sub>O (Sigma-Aldrich, technical grade), Tetraethyl orthosilicate (Merck, ≥99% purity), and NH<sub>4</sub>H<sub>2</sub>PO<sub>4</sub> (Merck, ACS grade) were dissolved in deionized water, leading to the formation of a gel. This gel was subsequently dried at 80°C, followed by calcination at 800°C for 4 h. Using a tumbling mixer, the calcined material was then ball-milled in an ethanol medium with zirconia milling balls measuring 3 and 5 mm. Once milled, the powder was dried and compacted to form 13 mm diameter cylindrical pellets at 100 MPa or directly exposed to a sintering process at 1260°C for 6 h. Post-sintering, any larger agglomerates were manually reduced using a mortar grinder.

NaTFSI (Solvionic, France) as well as the dispersion of Na<sub>3.4</sub>Zr<sub>2</sub>Si<sub>2.4</sub>P<sub>0.6</sub>O<sub>12</sub> in cross-linked PEO (bought from Alroko GmbH) was investigated. PEO cross-linking was realized via UV irradiation of *Bis(2,4,6-trimethylbenzoyl)-phenylphosphineoxide* (Irgacure819, BASF) which was dissolved in PEO.

The number of repetitions of PEO monomer units is about 230 units, and the average molecular weight  $M_w = 100$  kg/mol with a polydispersity ( $M_w/M_n$ ) = 2 ( $M_n$ : number related average molecular weight). The solid polymer and composite electrolytes were prepared by tape-casting the solution onto a PTFE sheet. The solvent Acetonitrile (Anhydrous, Sigma-Aldrich) was used for slurry preparation and subsequent tape casting. The solvent was stored under an argon atmosphere and further dried over molecular sieves. The solvent evaporated at room temperature after tape-casting the slurry onto a PTFE sheet. After evaporation, the solid polymer/ceramic composite electrolytes were dried under vacuum at 80°C inside the vacuum chamber attached to the glovebox for at least 20 h.

To quantify any residual solvent in the electrolyte, the samples were heat treated for different times (4 h, 8 h, 24 h, 48 h) inside the vacuum chamber at the abovementioned conditions. The samples were weighted on a precision scale before and after the heat treatment. A correlation between the duration of heat treatment and weight loss due to solvent evaporation could not be established. While this does not prove that no residual solvent is still inside the electrolytes, the amount still left inside is relatively low.

Scanning electron microscopy (SEM, supplementary information) also was applied to investigate the composite electrolytes. Top-view and cross-section observations revealed that the NaSICON particles are homogeneously distributed in the polymer electrolyte. NMR results on PEO with 50% (weight)  $\text{Na}_{3.4}\text{Zr}_2\text{Si}_{2.4}\text{P}_{0.6}\text{O}_{12}$  and on  $\text{PEO}_{20}\text{NaTFSI}$  (with  $n = 20$ , defined as  $n = [\text{EO units}]/[\text{Na}]$ ), show that the PEO mobility influences the ion mobility.

## 2.2 Experimental

### 2.2.1 NMR Experiments: Background and Pulse Sequences

Different NMR pulse sequences (Figure 1) were employed to investigate the transverse relaxation of the central ( $m_z: -1/2 \leftrightarrow 1/2$ ) and the satellite transitions ( $-3/2 \leftrightarrow -1/2$ ,  $3/2 \leftrightarrow 1/2$ ) [42], whereby mainly low-frequency fluctuations of interactions in the range of kHz determine transverse relaxation.  $^{23}\text{Na}$ -NMR measurements were performed using the pulse sequence parameters in Table 1. The pulse sequences differ in their refocusing properties, leading to potentially different transverse relaxation rates. This approach allows additional insight into the ion mobility in solid-state electrolytes. In short, static magnetic interactions are refocused in a Hahn echo (HE) experiment. In contrast, the solid echo (SE) is known to refocus interactions bilinear in the spin quantum number [42-44], namely quadrupolar and dipolar interactions. The  $\pi/2$ - $\beta$  experiment (PB) is known to refocus the magnetization of satellite transitions, leading to a maximum in echo amplitude at  $\beta = 64^\circ$  [38, 45, 46]. For the present case, the optimized version is the quadrupolar echo (QE), where the quadrupolar transients are diminished due to an optimized refocusing pulse ( $\eta$ ) and a dedicated phase cycle [47-49] (Table 1). The NMR signals are, therefore, differently weighted, which also shows up in the dependence of the signal integral on the echo time  $\tau$ . The differences thus reflect the respective contributions of magnetic interactions and interactions bilinear in the nuclear spin. This is true for static interactions, while the fluctuating interactions need a more detailed consideration of the respective time scales of fluctuations and experiments. The theoretical description and the relevant time scales of the fluctuations can be found for example in references [43, 44].

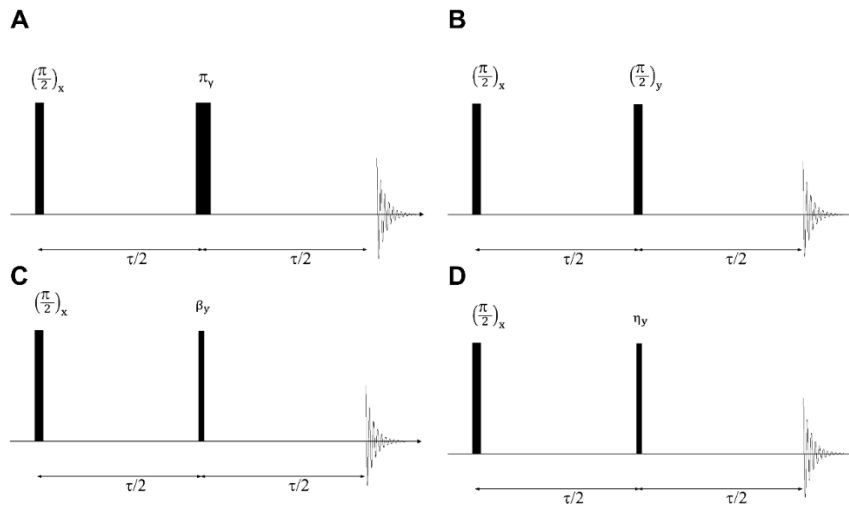


**Figure 1** Pulse sequences for transverse relaxation: Hahn-echo (A), solid-echo (B),  $\pi/2 - \beta$  experiment (C) and quadrupolar echo (D), the refocusing properties depend on the second rf-pulse and the phase cycle [50].

**Table 1** Parameters of the applied  $^{23}\text{Na}$ -NMR-experiments on SIB electrolytes.

	Hahn echo (HE)	Solid echo (SE)	$\pi/2 - \beta$ experiment, $\beta = 64^\circ$ (PB)	Quadrupolar echo (QE)
Temperature $T$ [K]	[297, 407]			
$90^\circ$ Pulse	7 $\mu\text{s}$ @ 20 W for NaTFSI, PEO <sub>20</sub> + NaSICON + NaTFSI and PEO <sub>20</sub> + NaTFSI, 18.25 $\mu\text{s}$ @ 11.75 W for Na <sub>3.4</sub> Zr <sub>2</sub> Si <sub>2.4</sub> P <sub>0.6</sub> O <sub>12</sub> , 11 $\mu\text{s}$ @ 20 W for PEO + NaSICON, respectively optimized			
Averages	[8, 20]			
Repetition time $T_R$ [s]	[1, 5]			
Echo time $\tau$ [ $\mu\text{s}$ ]	[65, 5646]	[47, 5627]	[62, 5622]	[43, 3027]
phase cycle: Preperation	[x, y, -x, -y]	[x, -y, -x, y, x, -y, -x, y]	[x, -y, -x, y, x, -y, -x, y]	[x, x, x, x, y, y, y, y, -x, -x, -x, -x, -y, -y, -y, -y]
Refocussing	[x, x, x, x, y, y, y, y, -x, -x, -x, -x, -y, -y, -y, -y]	[-y, -x, y, x, y, x, -y, -x]	[-y, -x, y, x, y, x, -y, -x]	[x, y, -x, -y, x, y, -x, -y, x, y, -x, -y, x, y, -x, -y]
Acquisition	[x, -y, -x, y, -x, y, x, -y]	[-y, -x, y, x, -y, -x, y, x]	[-y, -x, y, x, -y, -x, y, x]	[-y, y, -y, y, -x, x, -x, x, y, -y, y, -y, x, -x, x, -x]

Echo times were incremented in the given ranges (Table 1) to measure the transverse magnetization relaxation decays, i.e. the rates, as a function of  $T$ . Care was taken to measure the decays down to the noise level while not neglecting the fast-relaxing contributions.  $^1\text{H}$ -NMR FID's were measured in addition to correlate the PEO polymer mobility to the observations of  $^{23}\text{Na}$  in CPE. The following parameters were used for  $^1\text{H}$ :  $90^\circ$  pulse  $9.8 \mu\text{s}$  @  $11 \text{ W}$  with a repetition time of 3-5 s. 16 averages were added, and  $T$  was in the range of 300-407 K.

### 2.2.2 Raw Data Processing

The measured NMR raw data must be condensed and modeled to reveal interesting material parameters. The transverse magnetization decays were obtained by numerical integration of the spectra. The thus determined amplitudes as a function of echo time,  $A(\tau)$ , were modeled by either exponential, Gaussian, or combined functions depending on the properties of the decays. For liquids, the transverse relaxation rates  $R_2$  are most often obtained by fitting exponential functions to the data:

$$A(\tau) = A \exp(-R_{2E}\tau) \tag{1}$$

The transverse magnetization decays follow not necessarily an exponential decay in solids but instead adopt a Gaussian shape [43, 44]:

$$A(\tau) = A \exp(-(R_{2G}\tau)^2) \tag{2}$$

The choice of the model in the present case was not only determined by the numerical accuracy but by the interpretability, the appearance, and the shape of the decays (Figure 2). Depending on the pulse sequence, the measured data were modeled accordingly, most often by functions with two contributions. The subscripts indicate the respective mathematical function (E or G). A slight offset was allowed in all cases which, strictly speaking, is wrong, but allowed a numerically perfect description of the measured magnetization decays. Please note that temperature and the named NMR pulse sequences span the parameter field for the investigations of the solid electrolytes.

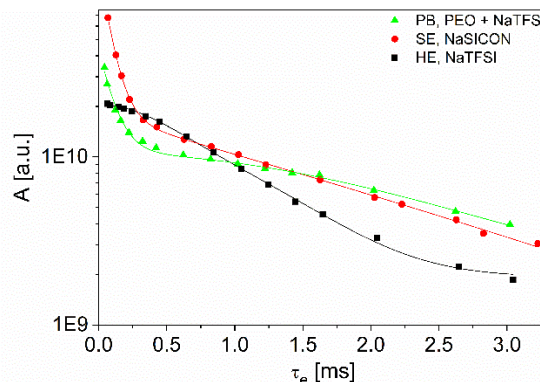


**Figure 2** Exemplary magnetization decays of the sodium electrolytes as measured by PB, SE, and HE at 327 K. The shape of the decays reflects the fluctuating spin interactions at the given refocussing properties of the pulse sequences. Biexponential (SE, NaSICON) as well as bi-Gaussian (HE, NaTFSI) and mixed decay functions (PB, PEO + NaTFSI) were used.

### 2.3 Models for NMR Transverse Relaxation and Line Width as a Function of Temperature

The NMR characteristics transverse relaxation rates  $R_2$  and line width  $\delta\nu$  are known to reflect material properties in the low-frequency range of fluctuations. They are often recorded as a function of  $T$ . Already in the frame of relaxation theory by Bloembergen, Pound, and Purcell [42, 51], the measured parameters were modeled in terms of magnetic and quadrupolar interactions, which is the basis for observing reorientation, hopping, and other phenomena like phase transitions. The corresponding equations are sketched in the following for 3D and 2D fluctuations.

In general,  $^{23}\text{Na}$   $R_2$  is the sum of fluctuating quadrupolar and magnetic contributions [42, 52-54]. Examples of the latter are fluctuations of chemical shift anisotropy, paramagnetic contributions, and homo- and heteronuclear dipolar interactions. As the time scales of fluctuations are in the focus rather than the details of nuclear spin interactions, we summarize the magnetic interactions in an effective parameter  $\Delta\omega_M$ . The quadrupolar interactions are summarized in the corresponding parameter  $\Delta\omega_Q$ . The transverse relaxation rate can then be modeled considering the contributions of fluctuations in the frequency range of line width  $\Delta\omega$ , of Larmor frequency  $\omega_L$  and  $2\omega_L$ :

$$\begin{aligned} R_2 &= R_{2M} + R_{2Q} \\ &= \frac{1}{40} \Delta\omega_M^2 [3J(\omega_L, \tau_c) + 4J(\Delta\omega, \tau_c)] + \frac{3}{40} \Delta\omega_Q^2 \left[ \frac{9}{5} J(\Delta\omega, \tau_c) + 8J(\omega_L, \tau_c) + \frac{31}{5} J(2\omega_L, \tau_c) \right] \\ &= aJ(\Delta\omega, \tau_c) + bJ(\omega_L, \tau_c) + cJ(2\omega_L, \tau_c) \end{aligned} \quad (3)$$

As the  $^{23}\text{Na}$  spectra of the investigated samples were rather unspecific and broad, the magnetic and quadrupolar interactions can hardly be quantified separately. This fact led to the less specific formulation of equation (3) focusing on the correlation time  $\tau_c$ . This approach nevertheless allows the determination of the time scales, i. e., the  $^{23}\text{Na}$  mobility: The time scales of the interaction's fluctuations are given by the spectral densities  $J(\omega, \tau_c)$  at a frequency  $\omega$ .  $J(\omega, \tau_c)$  is chosen as a Lorentzian function for 3D fluctuations:

$$J(\omega) = \frac{2 \tau_c}{1 + (\omega\tau_c)^2} \quad (4)$$

In the case of dominantly 2D interaction fluctuations or 2D hopping, the spectral density is given by the following equation ([38, 40] and references therein), while  $1 < \beta < 2$ :

$$J(\omega) = \tau_c \ln \left( 1 + \frac{1}{(\omega\tau_c)^\beta} \right) \quad (5)$$

Often, fluctuations in solids are modeled as thermally activated, and an Arrhenius approach with an activation energy  $\Delta E_a$  consequently describes the correlation times:

$$\tau_c = \tau_{c0} \exp \frac{\Delta E_a}{k_B T} \quad (6)$$

The thermal energy  $k_B T$  is given by the Boltzmann constant  $k_B$  and the absolute temperature  $T$ .  $\Delta E_a$  is a material-specific quantity that describes the energy barrier for the statistical hopping of ions [38]. The processes are also named solid-state diffusion to be distinguished from Brownian motion or diffusion in gases and liquids. A solid-state diffusion coefficient is calculated from the correlation

time by introducing or assuming a typical, relevant length scale. According to the Einstein-Smoluchowski equation [55], the solid-state diffusion coefficient  $D$  is given by

$$D = \frac{\langle x^2 \rangle}{2d\tau_c} \quad (7)$$

and intrinsically is a function of  $T$ . Within that model,  $\tau_c$  is assumed to be thermally activated, so is  $D$ , too. In the case of ordered substances like crystals, the energetically favored positions of ions in the crystal lattice are known. Therefore, the hopping length  $\langle x^2 \rangle$  and the hopping's dimensionality  $d$  can be deduced from the crystal's morphology. In the case of disordered structures and various interstitial sites of ions, an estimation is made to calculate at least the order of magnitude of  $D$ .

Line width  $\delta\omega = 2\pi \delta\nu$  is easily measurable in wide-line NMR spectroscopy, which reflects mobility. This fact is often referred to as motional narrowing, while a rigid lattice value is observed at low  $T$ . Several models are known, and one of them was applied to the data [42]. The following implicate equation describes the  $T$  dependence of  $\delta\omega(T)$ :

$$\delta\omega(T)^2 = \delta\omega'^2 \arctan(\alpha\delta\omega(T)\tau_c(T)) + \delta\omega''^2 \quad (8)$$

$\delta\omega''$  is the line width (in [rad/s]) at high temperatures, while  $\delta\omega'$  corresponds to the rigid lattice line width ( $T \rightarrow 0$  K) irrespective of the interaction leading to line broadening.  $\alpha$  is a numerical factor in the order of 1, which is introduced to compensate for inaccuracies in determining the line width mainly in the dynamic range of change in  $\delta\omega$ . This model was successfully applied to NMR line width measurements on diverse solid materials and broadening mechanisms, for example,  $\text{Rb}_4\text{C}_{60}$ ,  $\text{Rb}_3\text{C}_{60}$ ,  $\text{Li}_2\text{ZrO}_3$ ,  $\text{LiAlO}_2$ , and  $\text{K}_4\text{C}_{60}$  [27, 39, 52, 53, 56-58]. Other models leading to similar results are used, for example in [59, 60]. Further information can often be obtained by line shape analysis and 2D exchange experiments. However, in the present case, unstructured spectra were observed.

### 3. Results & Discussion

#### 3.1 NaSICON $\text{Na}_{3.4}\text{Zr}_2\text{Si}_{2.4}\text{P}_{0.6}\text{O}_{12}$ and NaTFSI: $\text{Na}^+$ Ions Studied by Wide-Line NMR

##### 3.1.1 Line Width

$^{23}\text{Na}$  wide-line NMR provided insight into ion mobility [28]. Two NaSICON samples of  $\text{Na}_{3.4}\text{Zr}_2\text{Si}_{2.4}\text{P}_{0.6}\text{O}_{12}$  (powder and pressed into pellets) were investigated.  $\delta\nu$ , defined as full width at half height, decreased with increasing  $T$ , indicating motional narrowing (Figure 3). The values of the differently processed  $\text{Na}_{3.4}\text{Zr}_2\text{Si}_{2.4}\text{P}_{0.6}\text{O}_{12}$  are identical within the experimental error, and the modeling of the data with equation (6) describes the data (black line) well. A small deviation occurs in the temperature range [310, 330] K, which was also observed for  $\text{Na}_{3.4}\text{Sc}_2(\text{SiO}_4)_{0.4}(\text{PO}_4)_{2.6}$  in [28]. The modeling reveals, assuming thermal activation of the line narrowing, an activation energy of  $\Delta E_a = 0.34$  eV at  $\tau_{c0} = 1$  ns in a similar range than found in electro-impedance spectroscopy [61].

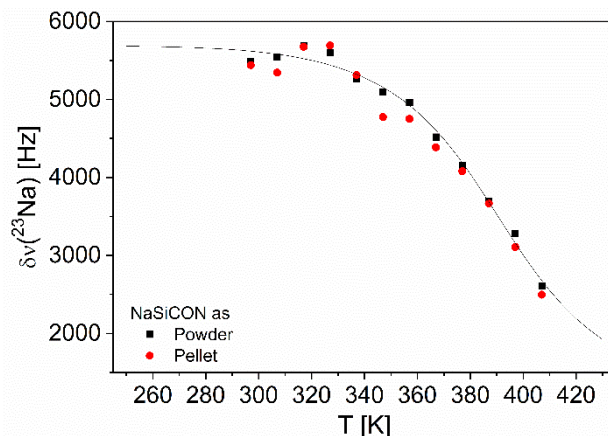


**Figure 3** Temperature dependence of  $^{23}\text{Na}$ -NMR line width  $\delta\nu(T)$  of the NaSiCON  $\text{Na}_{3.4}\text{Zr}_2\text{Si}_{2.4}\text{P}_{0.6}\text{O}_{12}$  in the form of powder and in the form of pellets, which is almost identical and independent of mechanical preparation. The black line represents the description by equation (6).

Compared to Li compounds [29, 37-40], line narrowing occurs at higher temperatures, indicating significantly slower mobility already observable in the raw data and, therefore, independent of modeling. As the solid-state diffusion coefficient is an essential parameter in simulations, we deduce from the data the following values: at room temperature, the line width is almost in the rigid value regime, indicating that the method became insensitive to the slow motions, the extrapolated diffusion coefficient is therefore relatively small:  $D(297\text{ K}) = 3.6 \times 10^{-17}\text{ m}^2/\text{s}$ . Around 350 K, the maximum of  $R_2$  (see below),  $D(350\text{ K}) = 2.9 \times 10^{-16}\text{ m}^2/\text{s}$ , whereas at 385 K, the upper range of measured temperatures,  $D(385\text{ K}) = 7 \times 10^{-16}\text{ m}^2/\text{s}$ .  $D$  was calculated based on thermal activation and 2D hopping.

The situation is different for NaTFSI,  $\delta\nu$  only weakly depends on  $T$  in the investigated  $T$  range:  $\delta\nu$  decreases from 2.7 kHz at 297 K to 2.6 kHz at 410 K, a determination of  $\Delta E_a$  is therefore hardly possible based on these data.

### 3.1.2 Transverse Relaxation

$^{23}\text{Na}$  transverse relaxation rates were measured on the two  $\text{Na}_{3.4}\text{Zr}_2\text{Si}_{2.4}\text{P}_{0.6}\text{O}_{12}$  samples by the mentioned NMR pulse sequences A-C (Figure 1, Table 1) and of NaTFSI by A-D (Figure 1, Table 1) to investigate the relaxation paths of  $^{23}\text{Na}$  magnetization. The aim is to get insight into  $\text{Na}^+$  mobility in these substances as a function of  $T$ .

Firstly, the relaxation results on the two differently prepared  $\text{Na}_{3.4}\text{Zr}_2\text{Si}_{2.4}\text{P}_{0.6}\text{O}_{12}$  samples are summarized in Figure 4 and Figure 5. The magnetization decay measured with the parameters in Table 1 were analyzed by exponential decay functions (equation (1)). Fit parameters are the amplitudes  $A_1$  and  $A_2$  as well as the two relaxation rates  $R_{2, iE}$ .  $R_{2, 1E}$  thereby describes the more significant part of magnetization given by  $A_1$ . It is a function of  $T$  with a maximum around 350 K for all three pulse sequences (HE, SE, PB), which indicates that the ion mobility changes with  $T$  in the fluctuation range of several kHz, in which  $R_2$  is sensitive. Interestingly, the amplitude ratio  $A_1/(A_1 + A_2)$  is nearly  $T$ -independent. At the same time,  $R_{2, 2E}$  representing the more slowly relaxing and less intense part of the magnetization decay, increases with  $T$ . This unusual behavior is a first indication

of an additional ion mobility or hopping process, which might appear at even higher temperatures in the transverse relaxation rates.

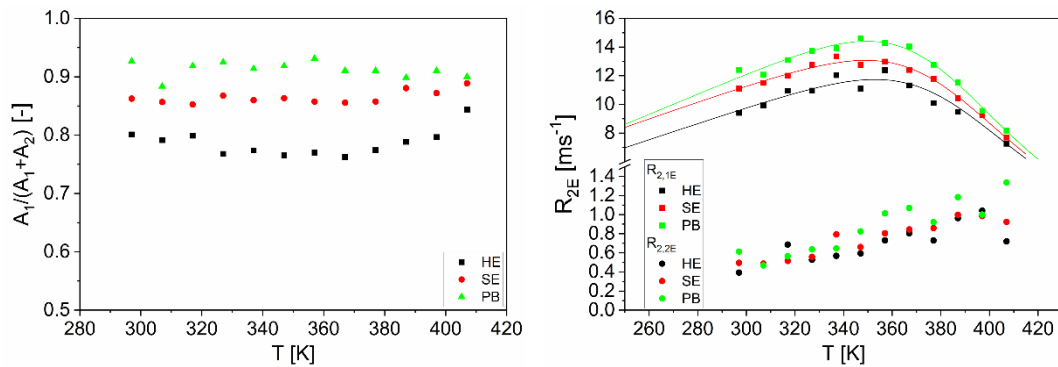


**Figure 4** NaSICON  $\text{Na}_{3.4}\text{Zr}_2\text{Si}_{2.4}\text{P}_{0.6}\text{O}_{12}$  (powder)  $^{23}\text{Na}$  transverse relaxation rates as deduced from magnetization decays by biexponential data modeling. Left: The fraction  $A_1/(A_1 + A_2)$  of the fast-relaxing component  $R_{2,1E}$  depends on the refocussing properties but appears approximately constant for  $T < 380$  K. Right: The  $T$ -dependence of both components  $R_{2,iE}$  is similar for the three sequences HE, SE, and PB.  $R_{2,1E}$  was modelled (lines), while  $R_{2,2E}$  increased approximately linear with  $T$ .

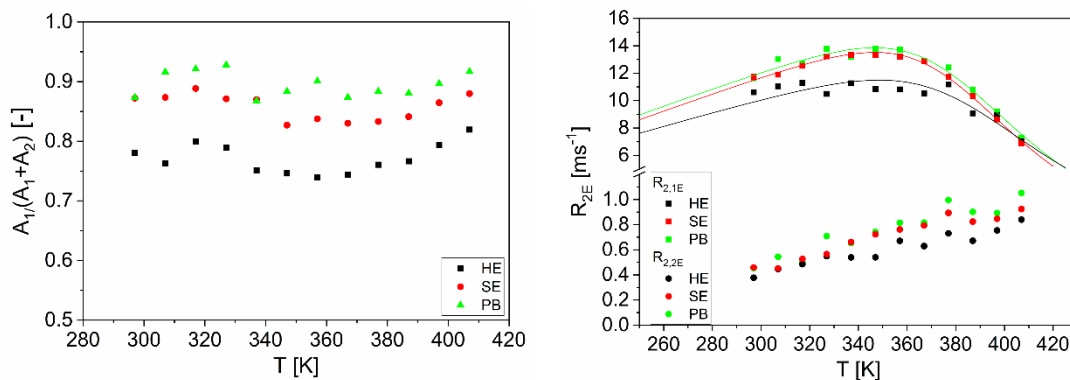


**Figure 5** NaSICON  $\text{Na}_{3.4}\text{Zr}_2\text{Si}_{2.4}\text{P}_{0.6}\text{O}_{12}$  (pellet)  $^{23}\text{Na}$  transverse relaxation rates as deduced from magnetization decays by biexponential data modelling. Left: Amplitude ratio of the fast relaxing component, right: The  $T$ -dependence of  $R_{2,iE}$  is similar to that in Figure 4 and was modelled by equations (3)-(7).

$R_{2,1E}$  were modeled using a linear combination of equations (3) and (8), including a weighting factor. This is due to the fact that a plateau of relatively large transverse relaxation rates was measured at low temperatures, similar to the findings in  $\delta\nu_c(T)$  (Figure 3), which was also observed in  $^7\text{Li}$ -NMR on  $\text{Li}^+$  in graphite. This fact led to an empirical extension of the established relaxation model to adequately describe the measured data. The weighting factor depends on the refocussing properties of the pulse sequences.

In the case of powder, the model delivers  $\Delta E_a$  and  $\tau_{c0}$  for HE: 0.64 eV, 0.1 ps; SE: 0.63 eV, 0.1 ps; and PB: 0.64 eV, 0.1 ps when assuming 2D jumps with an exponent  $\beta$  of 1.06-1.07 (equation (5)). The numbers indicate - as already do the measured data points - that the same  $\text{Na}^+$  hopping

processes in  $\text{Na}_{3.4}\text{Zr}_2\text{Si}_{2.4}\text{P}_{0.6}\text{O}_{12}$  (powder) is observed in all  $R_2$  measurements - irrespective of the different weighting of magnetic and quadrupolar interactions. From  $\tau_c(T)$  with an average jump distance  $\langle x^2 \rangle = 3.5$  nm deduced from the crystal lattice [31], the solid-state diffusion coefficients of  $\text{Na}^+$  in  $\text{Na}_{3.4}\text{Zr}_2\text{Si}_{2.4}\text{P}_{0.6}\text{O}_{12}$  (powder) can be calculated within the model of thermally activated 2D hopping ( $d = 2$ , equation (7)).

At  $T = 350$  K, the solid-state diffusion coefficient is in the range  $D(350 \text{ K}) = 1.9 \times 10^{-16} \text{ m}^2/\text{s}$  (HE) -  $D(350 \text{ K}) = 2.3 \times 10^{-16} \text{ m}^2/\text{s}$  (PB) (2D), for 3D hopping the following range was found:  $D(350 \text{ K}) = 1.3 \times 10^{-15} \text{ m}^2/\text{s}$  (SE) -  $3.3 \times 10^{-15} \text{ m}^2/\text{s}$  (HE). The values are small and highly dependent on  $T$  due to the model of thermal activation. However, we want to point out that the peaks in  $R_2$  are observed at relatively high temperatures. The estimation according to the BPP model (3D) would result in  $D(350 \text{ K}) = 1.6 \times 10^{-15} \text{ m}^2/\text{s}$ , which confirms the modeling of  $R_2(T)$ .

Usually,  $R_1$  is measured.  $R_1$  on the very same NaSICON (progressive saturation recovery) shows a peak maximum around the same temperature of 350 K, peak modeling results in  $\Delta E_a = 0.35$  eV (2D), 0.24 eV (3D) and  $\tau_{c0} = 0.01$  ps (2D), 0.4 ps (3D). Solid-state diffusion coefficients are then:  $D(300 \text{ K}) = 3.5 \times 10^{-12} \text{ m}^2/\text{s}$  (2D),  $4 \times 10^{-12} \text{ m}^2/\text{s}$  (3D), and at the peak maximum  $D(350 \text{ K}) = 2.9 \times 10^{-11} \text{ m}^2/\text{s}$  (2D),  $1.5 \times 10^{-11} \text{ m}^2/\text{s}$  (3D). These values are in the commonly observed range of solid-state diffusion coefficients. The fact that both  $R_1$ , being most sensitive to fluctuations at the Larmor frequency, and  $R_2$ , most sensitive in the kHz range, i.e., line width, show relaxation peaks in the same temperature range leads to the conclusion that two different processes of ion mobility were observed. This observation may hint at frequency distributions of fluctuations rather than one well-defined and unique hopping rate of  $\text{Na}^+$  in  $\text{Na}_{3.4}\text{Zr}_2\text{Si}_{2.4}\text{P}_{0.6}\text{O}_{12}$ . As the transverse relaxation approach is not established and promises additional insights, it will be pursued in the following sections of this paper, showing the impact of low-frequency fluctuations.

The NaSICON  $\text{Na}_{3.4}\text{Zr}_2\text{Si}_{2.4}\text{P}_{0.6}\text{O}_{12}$  (pellet) data resulting from modeling are compared to the findings on the powder:  $E_a$  and  $\tau_{c0}$  are for HE: 0.6 eV, 0.1 ps; SE: 0.66 eV, 0.1 ps; PB: 0.64 eV, 0.1 ps, assuming 2D jumps with an exponent  $\beta$  of 1.02-1.06 (equation (5)). The solid-state diffusion was calculated as a function of  $T$ . At  $T = 350$  K,  $D(350 \text{ K}) = 1 \times 10^{-16} \text{ m}^2/\text{s}$  (SE) -  $D(350 \text{ K}) = 7.8 \times 10^{-16} \text{ m}^2/\text{s}$  (HE) (2D) (3D:  $D(350 \text{ K}) = 4.5 \times 10^{-16} \text{ m}^2/\text{s}$  (SE) -  $6.5 \times 10^{-16} \text{ m}^2/\text{s}$  (HE)). These values are identical within the experimental errors to those for  $\text{Na}_{3.4}\text{Zr}_2\text{Si}_{2.4}\text{P}_{0.6}\text{O}_{12}$  (powder). To complete the modelling, 3D hopping was assumed, too. The measured data could also be modeled numerically well, however, with physically questionable parameters, overall indicating 2D hopping: The activation energies for 3D hopping would be in the order of magnitude of 0.33 eV,  $\tau_{c0}$ , however, would be in the range [285, 800] ps, which is orders of magnitude larger than usually observed. The line width contribution would increase from a minor importance of  $1 \times 10^{-7}$  (2D) to 0.3 (3D), a questionable value. In consequence, the diffusion coefficients differ significantly. The data, therefore, can also be interpreted as a hint on the hopping's dimensionality, which is 2D in the case of  $\text{Na}_{3.4}\text{Zr}_2\text{Si}_{2.4}\text{P}_{0.6}\text{O}_{12}$ .

In summary, the NMR parameters line width and transverse relaxation do not show a significant influence of mechanical treatment on the nanoscale hopping of  $\text{Na}^+$  in  $\text{Na}_{3.4}\text{Zr}_2\text{Si}_{2.4}\text{P}_{0.6}\text{O}_{12}$ . The  $\text{Na}^+$  fluctuations, however, show up in the measurements, and corresponding data treatment and modeling reveal the characterizing quantities.

As already found for the  $^{23}\text{Na}$  line width, the transverse relaxation behavior of NaTFSI differs from that of  $\text{Na}_{3.4}\text{Zr}_2\text{Si}_{2.4}\text{P}_{0.6}\text{O}_{12}$ : The magnetization decays exhibit a significant Gaussian contribution, which is well known for and often found in crystalline solids [43, 44]. The decays were, therefore, modeled with either bi-Gaussian decay functions (equation (2)) or a sum of an exponential and a

Gaussian decay function. The relaxation rates (Figure 6) are labeled correspondingly. Please note that the shape of the decay depends on the refocusing properties. In addition to the pulse sequences A-C (Figure 1), the quadrupolar echo QE sequence (Figure 1, D) was used as quadrupolar transients were observed, which hampered data processing. These contributions could be significantly reduced in QE, resulting in decays describable by the bi-Gaussian function (equation (2)).

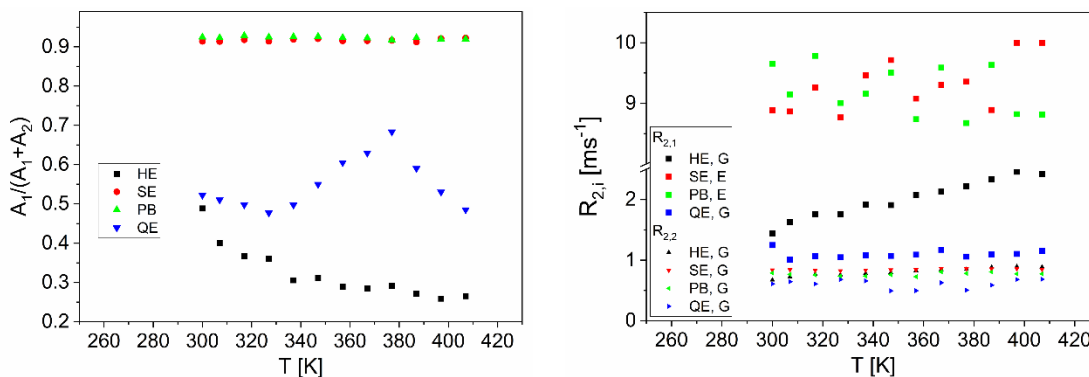


**Figure 6** NaTFSI <sup>23</sup>Na transverse relaxation rates: Left: fraction of the faster relaxing part as a function of temperature for the four pulse sequences, right: depending on the pulse sequence and its refocusing properties, exponential E and Gaussian G contributions were modeled and result in the corresponding relaxation rates.

The slower relaxing parts  $R_{2,2G}$  of the magnetization decays (Figure 6, right) are similar and roughly  $T$ -independent, while its fraction is  $T$ -dependent - most pronounced for QE and HE. The fast Gaussian contribution in HE  $R_{2,1G}$  is the only component showing a significant  $T$ -dependence. Instead, SE and PB magnetization decays are dominated by a fast exponential relaxation contribution in a similar range of values as observed for  $\text{Na}_{3.4}\text{Zr}_2\text{Si}_{2.4}\text{P}_{0.6}\text{O}_{12}$ . When comparing the relaxation decays of NaTFSI before and after the temperature cycle, differences were observed mainly in the fast-decaying part of the relaxation, indicating a reordering in NaTFSI on the nm length scale. The data show the complexity of NMR transverse relaxation on quadrupolar nuclei in solid state. The differences to the findings in  $\text{Na}_{3.4}\text{Zr}_2\text{Si}_{2.4}\text{P}_{0.6}\text{O}_{12}$  are noted in the present context. Both data sets provide the basis to get insight into the  $\text{Na}^+$  behavior in the solid-state electrolytes PEO + NaSICON, PEO + NaTFSI, and PEO + NaSICON + NaTFSI.

### 3.2 PEO + NaSICON, PEO + NaTFSI, and PEO + NaSICON + NaTFSI: Temperature Dependence of the NMR Parameters

Composite polymeric electrolytes based on PEO are currently being investigated to improve the mechanical properties of solid-state Na-electrolytes. In addition to the pure substances NaSICON  $\text{Na}_{3.4}\text{Zr}_2\text{Si}_{2.4}\text{P}_{0.6}\text{O}_{12}$  and NaTFSI mentioned above, the CPE PEO + NaSICON, PEO + NaTFSI, and PEO + NaSICON + NaTFSI were investigated. Here,  $\text{Na}_{3.4}\text{Zr}_2\text{Si}_{2.4}\text{P}_{0.6}\text{O}_{12}$  is abbreviated as NaSICON in the following. The comparison of the results reflects the structural changes with their impact on the respective fluctuations monitored at the sites of the ions by Na-NMR.

NaSICON and NaTFSI are now distributed in PEO polymeric networks with their own molecular dynamics. As the Na-containing ceramics and salts contain no <sup>1</sup>H according to the chemical formula,

neglecting possible impurities,  $^1\text{H}$ -NMR allows the investigation of the polymeric network of CPE. Thus,  $^{23}\text{Na}$ -NMR provides insight into  $\text{Na}^+$  mobility, and the combination of  $^1\text{H}$ - and  $^{23}\text{Na}$ -NMR finally allows the identification of factors determining the Na-NMR sensed fluctuations in the low-frequency range.

### 3.2.1 Line Width

First, we focus on the  $T$ -dependence of  $^1\text{H}$ - and  $^{23}\text{Na}$ -NMR line width  $\delta\nu$ , defined again as the full width at half height, measured on PEO + NaSICON (Figure 7).  $\delta\nu (^1\text{H})$  is sensitive to the molecular mobility of PEO: the slope of  $\delta\nu (^1\text{H}, T)$  changes significantly around 317 K. This mainly is due to molecular dynamics in the polymer network, which influences the line width via magnetic, mainly homonuclear dipolar interactions. This is confirmed by  $^1\text{H}$ -NMR measurements on pure PEO (Figure 7). The line width at 407 K  $\delta\nu (^1\text{H}, 407 \text{ K}) = 600 \text{ Hz}$  still is orders of magnitude broader than observed in liquids with the instrument vendor's specification of  $\delta\nu (^1\text{H}) = 0.28 \text{ Hz}$ . We, therefore, do not observe complete motional narrowing at 410 K for both PEO and PEO + NaSICON, similar to what was often observed and what is expected for a cross-linked polymer, f.e. references [62, 63].

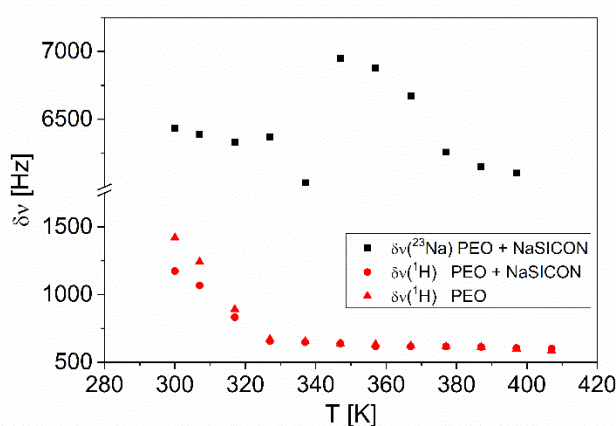


**Figure 7** PEO + NaSICON and PEO:  $^1\text{H}$  and  $^{23}\text{Na}$  line widths ( $\delta\nu (^1\text{H})$  and  $\delta\nu (^{23}\text{Na})$ ) as a function of  $T$ .  $\delta\nu (^1\text{H})$  reflects the transition in PEO structure evidenced by the steep slope around 317 K, while  $^{23}\text{Na}$  line width mainly reflects fluctuations of the quadrupolar interactions with a maximum around  $T = 350 \text{ K}$ . Please note this small difference in  $\delta\nu (^1\text{H})$  and  $\delta\nu (^{23}\text{Na})$  as well as the large difference to Figure 3.

In the  $T$ -window around 350 K,  $\delta\nu (^{23}\text{Na})$  peaks, which is an unusual behavior for NMR line width and clearly differs from the observation in Figure 3. As noted,  $\delta\nu (^{23}\text{Na})$  is sensitive to magnetic and quadrupolar interactions and their fluctuations. The data, especially the increase of  $\delta\nu (^{23}\text{Na})$  for  $T < 350 \text{ K}$ , indicate that the quadrupolar interactions cross the sensitive range of a few kHz of  $^{23}\text{Na}$  wide-line NMR. For  $T < 320 \text{ K}$ , the usual broadening is found. At  $T > 360 \text{ K}$ , partial motional averaging is observed while the line width is still high, especially when compared to pure NaSICON.

The observations in Figure 7 need to be compared to the line width of pure NaSICON (Figure 3), where a monotonous behavior was observed, leading to insight into the ion's mobility. In PEO + NaSICON, the peak around 350 K obscures this behavior.  $\delta\nu (^{23}\text{Na}, \text{PEO} + \text{NaSICON}) > \delta\nu (^{23}\text{Na}, \text{NaSICON})$  is valid for all  $T$  and leads to the interpretation that either additional relaxation paths are present in PEO + NaSICON or more likely, the environment of  $\text{Na}^+$  changed significantly in the PEO

matrix on the length scale of nm, i.e. the NaSICON structure deviates in PEO significantly from that of pure NaSICON and is most likely no longer describable by independent crystallites.

Furthermore, the findings on the CPE need to be compared. As already stated,  $\delta\nu(^1\text{H})$  is sensitive to the molecular mobility of PEO: the slope of  $\delta\nu(^1\text{H}, T)$  changes significantly around 317 K not only for PEO + NaSICON but also for PEO + NaTFSI and PEO + NaSICON + NaTFSI which was attributed to “melting” of the crystalline parts of PEO in this temperature range [64] resulting in an overall softening of the material. It should be noted that the 3D polymeric network does not melt in the usual thermodynamic sense of a solid becoming a liquid, but the ordering and the mobility of the polymer chains change, macroscopically resulting in softening. The similarity (Figure 8) to  $\delta\nu(^1\text{H}, T)$  in PEO + NaSICON leads to the conclusion that the critical temperature range of PEO molecular fluctuations differs not significantly for these CPE samples. However, when looking at the absolute values of  $\delta\nu(^1\text{H})$ , differences become evident:  $\delta\nu(^1\text{H})$  of PEO + NaSICON levels off for  $T > 330$  K around 600 Hz, whereas a more steep slope is observed for PEO + NaTFSI (leveling off at 350 Hz) and PEO + NaSICON + NaTFSI (ending around 800 Hz). As  $^1\text{H}$  dipolar couplings are known to depend on and decrease with temperature, the line width indicates molecular dynamics. Residual dipolar couplings are still observed at high temperatures [62, 63]. The observations point out that the molecular dynamics of PEO is influenced by the Na ceramics/salt significantly, while the temperature range of the PEO mobility transition itself is not.

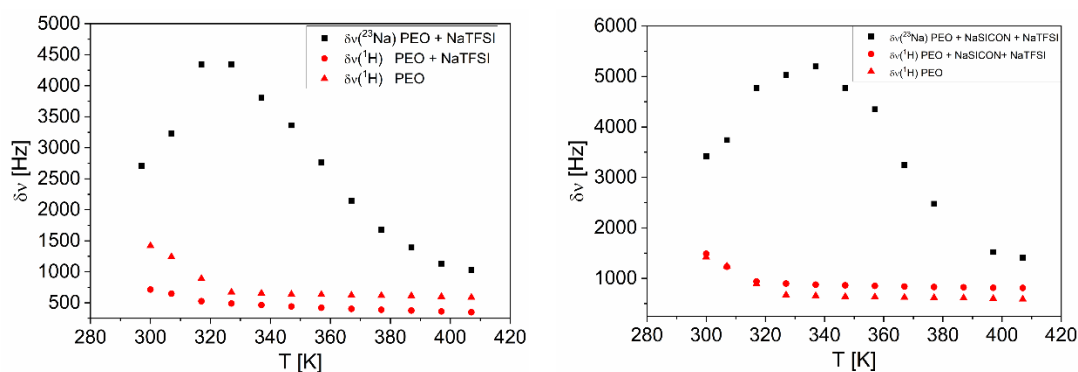


**Figure 8** Left: PEO + NaTFSI:  $^1\text{H}$  and  $^{23}\text{Na}$  line width ( $\delta\nu(^1\text{H})$  and  $\delta\nu(^{23}\text{Na})$ ) as a function of  $T$ . Again,  $\delta\nu(^1\text{H})$  reflects the transition in PEO mobility. In contrast,  $\delta\nu(^{23}\text{Na})$  mainly reflects fluctuations of the quadrupolar interactions. Right: PEO + NaSICON + NaTFSI:  $\delta\nu(^1\text{H})$  and  $\delta\nu(^{23}\text{Na})$  as a function of  $T$ . A similar  $T$ -dependence is observed, while the peak in  $\delta\nu(^{23}\text{Na})$  is considerably broader.

In analogy to the finding for pure salts, the  $^{23}\text{Na}$  wide-line NMR of PEO + NaTFSI differs significantly from that of PEO + NaSICON. In addition,  $\delta\nu(^{23}\text{Na}, \text{PEO} + \text{NaTFSI})$  differs from the quasi- $T$ -independent  $\delta\nu(^{23}\text{Na}, \text{NaTFSI})$ . A clear peak around 330 K was observed, and the dynamic range of the line width was larger. Most likely, quadrupolar interactions change near the PEO mobility transition, which becomes evident in the relatively large line width, while line narrowing occurs at large  $T$ .

The similarity in  $\delta\nu(^1\text{H}, ^{23}\text{Na}, T)$  for the three CPE PEO + NaSICON, PEO + NaTFSI, and PEO + NaSICON + NaTFSI is apparent (Figures 7 and 8), although the scales differ. The transition in  $^1\text{H}$ -PEO is around 317 K for all compounds, while  $\delta\nu(^{23}\text{Na})$  peaks around 325 K (PEO + NaTFSI) and 350 K

(PEO + NaSICON, PEO + NaSICON + NaTFSI). As this unusual peak occurs at lower temperatures for PEO + NaTFSI, we argue that the broader and more pronounced peak in PEO + NaSICON + NaTFSI can be interpreted as the sum of both contributions, NaTFSI and NaSICON, which act independently of each other but are significantly influenced by PEO. In the light of motional narrowing (equation (8)), a peak in line width is not expected. The observation thus indicates that the mobility transition of the PEO polymer matrix influences Na<sup>+</sup> sensed fluctuations, which become fast, i.e., the line shows partial motional averaging at high temperatures. Still, increased interactions are observed in the intermediate  $T$  range. In that sense, the Na<sup>+</sup> mobility of neither NaSICON nor NaTFSI is independent of the surrounding PEO network, which is also promoted by the attractive interaction between Na<sup>+</sup> and the oxygens of PEO. <sup>1</sup>H-NMR reflects the polymer mobility of the cross-linked PEO, which is attributed to the disordering of crystalline parts of the PEO network. The transition temperature is hardly affected by NaSICON and NaTFSI. However, the chain mobility is: NaSICON disturbs the ordering to a lower extent than NaTFSI, which is evident at low temperatures. At high temperatures, it becomes apparent that NaTFSI leads to broadening in <sup>1</sup>H spectra, while NaSICON does not, due to the particulate nature of NaSICON. In the case of PEO + NaTFSI + NaSICON, the dynamics of the PEO polymer shows a distinct behavior as observable in <sup>1</sup>H line width: While the fluctuations are similar to pure PEO at low  $T$ , the line narrowing is not as complete as for pure PEO at large  $T$ .

For an easier quantitative comparison of the findings on the different samples, a risky attempt was made to model the right-hand side of  $\delta v$  (<sup>23</sup>Na), i.e., for  $T > 330$  K. The fit parameters are summarized in Table 2 and reflect the data. Please note that the model in eq. 8 was established for motional narrowing but not for phase transitions and collective motion. The values need to be considered as rough estimates for easier comparability rather than as physically interpretable values.

**Table 2** Estimation of the activation energies and  $\tau_{c0}$  according to equation (8) from <sup>23</sup>Na line width.

	$\Delta E_a$ [eV]	$\tau_{c0}$ [ps]	$\delta\omega'$ [rad/s]	$\delta\omega''$ [rad/s]
NaSICON	0.35	1000	35176	6328
PEO-NaTFSI	0.41	50	28313	4366
PEO-NaTFSI-NaSICON	0.62	0.10	33837	7075

### 3.2.2 Transverse Relaxation

Also, <sup>23</sup>Na transverse relaxation in CPE differs significantly from the pure substances  $R_2$ . Again, PEO + NaSICON is discussed first. While peaks were observed for NaSICON,  $R_{2i}$  of PEO + NaSICON are almost flat (Figure 9); the indication of specific ion hopping is therefore not given in the measured transverse relaxation. In light of a variety of energetically similar sites in the polymeric network, these findings are not astonishing but a consequence of the CPE chemical properties. Please note, however, that a bi-exponential decay could no longer describe all the magnetization decays but by the sum of an exponential and a Gaussian decay with similar fractions. While the faster component is temperature independent within the experimental error, the slower part - now as Gaussian decay - shows a continuous increase similar to the findings for pure NaSICON, while the relative amplitude increased.

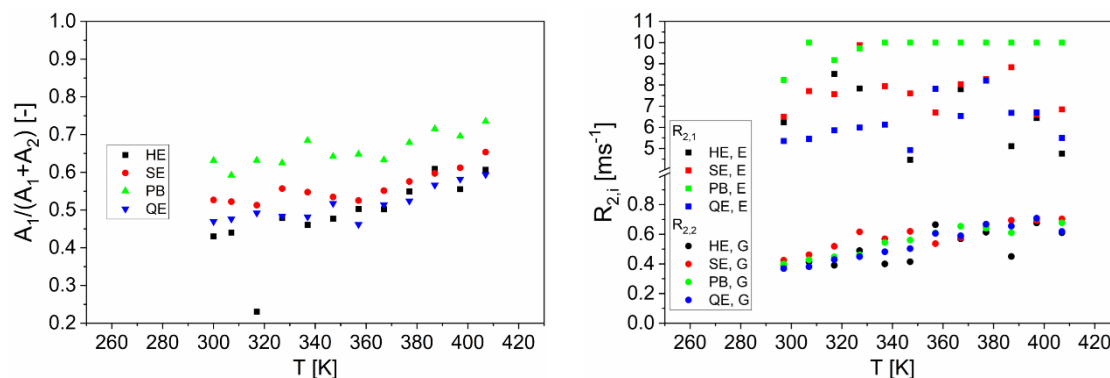


**Figure 9** PEO + NaSICON:  $^{23}\text{Na}$  transverse relaxation amplitudes (left) and rates (right) measured by the four pulse sequences (Figure 1 A-D) as a function of  $T$ . The two relaxation contributions E and G contribute to the magnetization decay with similar fractions. While the fast relaxation differs from NaSICON and is almost  $T$ -independent, the slower relaxation rate increases slightly but monotonically with  $T$  similar to the findings in pure NaSICON.

The situation again is different in PEO + NaTFSI (Figure 10): While in the pure substance NaTFSI transverse relaxation was unspecific, similar to  $^{23}\text{Na}$  line widths,  $R_{2,i}$  show pronounced temperature dependencies for the CPE. Please note that the decays were modelled by mixed functions except for the Hahn echo decay (HE). Apart from the relaxation rates deduced from QE, all other sequences measure peaks around 325 K. Modelling leads to activation energies  $\Delta E_a$  of 0.35-0.6 eV at  $\tau_{c0}$  of 0.01-1 ps (Table 3). Diffusion coefficients cannot reliably be calculated within the given model as the hopping distances are hardly known in a polymeric network such as cross-linked PEO. The fractions of fast and slower parts of the magnetization differ significantly in this case, which gives insight into the magnetic and quadrupolar interactions: HE refocuses the static magnetic interactions, while quadrupolar contributions lead to relaxation. Contrarily, QE refocuses quadrupolar interactions, which is extreme for PB. QE diminishes the contributions of quadrupolar transients, which agrees with the lack of peak in the fast-relaxing component of QE, which is still present for SE and PB. The observation leads to the interpretation that fluctuating electric field gradients are the dominant source of transverse relaxation in the measured temperature range. Attention should be paid to the fact that considerable Gaussian contributions were observed at low  $T$  in SE, PB, and QE, which usually indicate solid-state behavior:  $(A_2/(A_1 + A_2))$ , the amplitude fraction, decreases for PB and SE with  $T$  which again shows that fluctuating quadrupolar interactions are the cause of the observation.

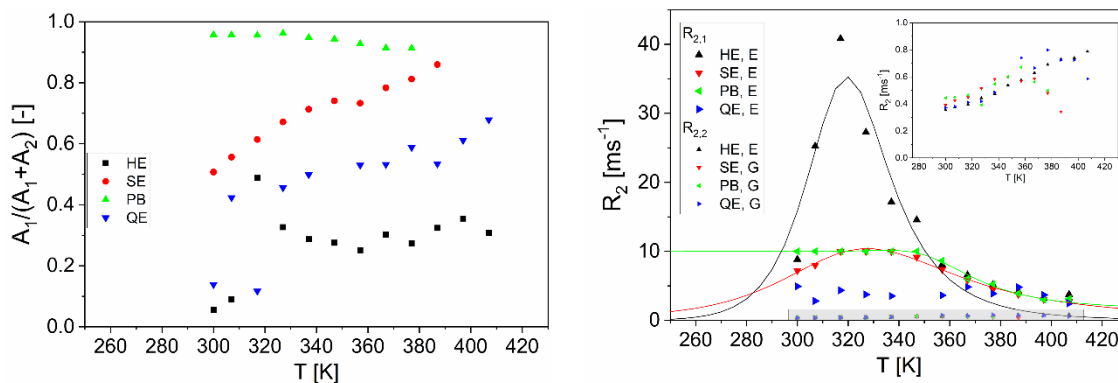


**Figure 10** PEO + NaTFSI:  $^{23}\text{Na}$  transverse relaxation measured by the four pulse sequences as a function of  $T$ : The amplitude fraction of the fast relaxation component (left) depends on the refocussing properties, as do the relaxation rates (right).  $R_2$  shows peaks for HE, SE, and partially PB, which were modeled in 3D (lines). The slowly relaxing components show mixed behavior (grey box; details are shown in the insert).

The slower part of relaxation shows a mixed behavior: HE increases monotonously, while SE, PB, and QE peak. No further modeling was made. The model describes the  $R_{2,1}$  data for HE, SE and PB sufficiently good. The important fit parameters are summarized in Table 3.

Finally, the CPE PEO + NaSICON + NaTFSI is discussed regarding the transverse relaxation rates (Figure 11). All magnetization decays except for QE could be described with a bi-exponential fit function resulting in the amplitudes  $A_1$  and  $A_2$  and the relaxation rates  $R_{2,1E}$  and  $R_{2,2E}$ . At the same time, QE is modeled as the sum of an exponential and a Gaussian decay. The faster relaxing QE component  $R_{2,1E}$  is approximately  $T$ -independent, and  $R_{2,2E}$  shows an increase, if not an onset of a peak in  $R_{2,2G}$  at  $T > 410$  K. This increase is also observed in  $R_{2,2E}$  measured by HE, SE, and PB. Peaks around 330 K were modeled, the resulting fit parameters are again summarized in Table 3.

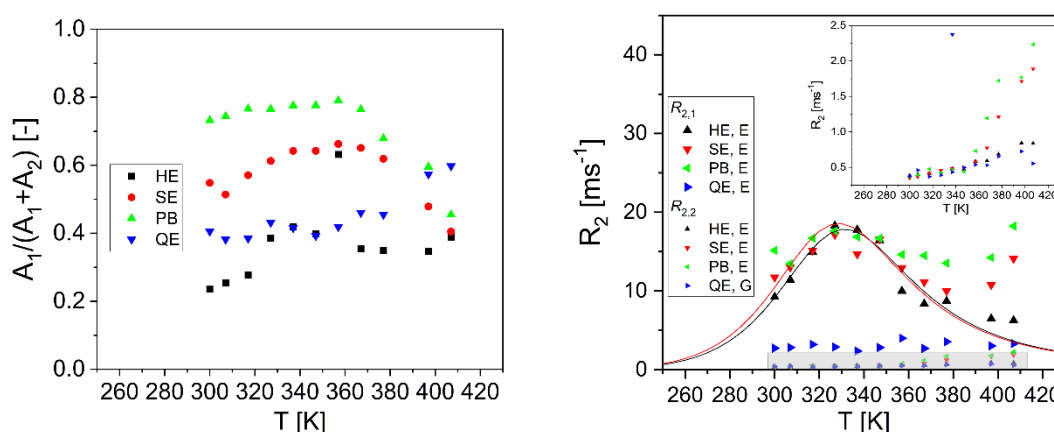


**Figure 11** PEO + NaSICON + NaTFSI: The fraction of the faster relaxing component ( $^{23}\text{Na}$ -NMR) is diverse for the four pulse sequences reflecting magnetic and quadrupolar contributions to the magnetization decays.  $^{23}\text{Na}$  transverse relaxation rates (right), measured by the four pulse sequences as a function of  $T$  and modeled by a bi-exponential or mixed magnetization decay, reveal ion mobility.

**Table 3** Fit parameters for the samples and pulse sequences: activation energies  $\Delta E_a$  and  $\tau_{c0}$  according to equation (8). The dimensionality of the better fit is marked in bold letters.

Sample	Pulse sequence	$\Delta E_a$ [eV]	$\tau_{c0}$ [ps]	$\Delta\omega$ [rad/s]	$W$ [-]	$\beta$ [-]
NaSICON (powder) $R_2$	<b>HE 2D</b>	0.64	0.1	68858	1.0E-07	1.07
	<b>SE 2D</b>	0.63	0.1	72152	1.0E-07	1.06
	<b>PB 2D</b>	0.64	0.1	76241	2.0E-03	1.07
	HE 3D	0.21	6694	91706	1.9E-01	-
	SE 3D	0.24	5095	54858	2.7E-01	-
	PB 3D	0.33	244	63367	3.2E-01	-
NaSICON (powder) $R_1$	<b>2D</b>	0.35	0.01	-	-	1.56
	<b>3D</b>	0.24	0.4	-	-	-
NaSICON (pellet) $R_2$	<b>HE 2D</b>	0.6	0.1	63196	1.0E-07	1.02
	<b>SE 2D</b>	0.66	0.1	73514	1.0E-07	1.06
	<b>PB 2D</b>	0.64	0.1	73962	1.0E-07	1.06
	HE 3D	0.35	285	45828	3.0E-01	-
	SE 3D	0.34	589	30000	3.2E-01	-
	PB 3D	0.32	796	35893	3.3E-01	-
PEO-NaTFSI $R_2$	HE 2D	0.70	0.01	11737	1.0E-10	2.00
	SE 2D	0.46	0.1	186112	1.6E-01	2.00
	PB 2D	0.70	0.1	3105	3.5E-01	2.00
	<b>HE 3D</b>	0.61	0.01	83066	2.0E-06	-
	<b>SE 3D</b>	0.35	1.0	605315	2.0E-07	-
	<b>PB 3D</b>	0.59	0.1	26279	3.5E-01	-
PEO-NaTFSI-NaSICON $R_2$	HE 2D	0.44	0.02	853014	1.0E-10	2.00
	SE 2D	0.44	1.0	698367	2.0E-06	1.00
	<b>HE 3D</b>	0.35	1.0	771223	1.0E-10	-
	<b>SE 3D</b>	0.35	1.0	799661	2.0E-06	-

As PEO undergoes a transition around 317 K, temperature cycles were performed to observe the reversibility of the CPE's thermodynamic state. While complete reversibility was observed for PEO + NaSICON + NaTFSI on the time scale of an NMR  $T$  cycle of several hours, PEO + NaSICON showed significantly different values in the back-cycle, which was assigned to the equilibration of the partially crystalline structures in PEO.

#### 4. Conclusions

Solid state Na electrolytes were investigated by wide-line NMR. Line width was quantified, and transverse relaxation was investigated by different pulse sequences. It became evident that the pure substances and the corresponding CPE with PEO as a cross-linked polymer differ considerably regarding ion mobility in the low-frequency range of kHz.  $^{23}\text{Na}$ -NMR sensed that PEO significantly influences fluctuations, and the corresponding NMR measures vary substantially for the investigated electrolytes in this low-frequency range. However, the segmental mobility of PEO changes in the same temperature range and is largely independent of the Na-containing species,

with signatures in the absolute values of  $^1\text{H}$  line width. This segmental mobility, however, shows up in  $^{23}\text{Na}$ -NMR and indicates that the  $^{23}\text{Na}$ -NMR sensed fluctuations depend on the state of the polymer matrix that embeds the ion conductor.

Fluctuations are usually analyzed in the MHz range (Larmor frequency) by NMR longitudinal relaxation. The findings in this paper prove the feasibility of exploring an additional frequency window for the characterization of solid-state electrolytes by line width and transverse relaxation. When possible, activation energies were deduced from the data in the order of 0.3 eV to 0.7 eV.

The combination with  $^1\text{H}$  line width reveals that the low frequency fluctuations monitored in  $^{23}\text{Na}$ -NMR sensed PEO molecular mobility in CPE. PEO retains its thermodynamic properties and only becomes softer. In contrast, the residual dipolar couplings, i.e., the  $^1\text{H}$ -line widths at high temperatures, are specific for the Na-containing material.  $\text{Na}^+$  transverse relaxation, instead, partially allows the determination of the thermal activation energies of ion mobility. Indications of the dimensionality of hopping result from modeling: 2D hopping appears appropriate in the case of the NaSiCON  $\text{Na}_{3.4}\text{Zr}_2\text{Si}_{2.4}\text{P}_{0.6}\text{O}_{12}$ , while the model with 3D hopping describes the data better for the investigated CPE.

## Acknowledgments

We thank S. Schuhmann for discussions and his kind cooperativeness. The current Pro<sup>2</sup>NMR members are highly appreciated for fruitful discussions and readiness to assist in the experimental work.

## Author Contributions

Conceptualization and methodology F.M., A.M., T.R., G.G.; sample preparation N.R., G.D., M.F.; data curation, investigation F.M., A.M., T.R., G.G.; resources, F.G., H.N., G.G.; visualization and writing-original draft preparation, F.M., A.M., G.G.; writing-review and editing, F.M., A.M., T.R., N.R., M.F., F.G., H.N., G.G.; supervision, funding acquisition H.N., G.G. All authors have read and agreed to the published version of the manuscript.

## Funding

The authors would like to thank the German Research Foundation (DFG) for financial support of the instrumental facility Pro<sup>2</sup>NMR. Furthermore, the authors thank the DFG for funding and support within GRK 2218 SiMET-Simulation of mechano-electro-thermal processes in lithium ion batteries, project number: 281041241. The "Bundesministerium für Bildung und Forschung" funded F. Gerbig within the project number 03XP0403D.

## Competing Interests

The authors have declared that no competing interests exist.

## Additional Materials

1. SEM Images of Composite Electrolytes, i.e. PEO + NaSiCON + NaTFSI.

## References

1. Janek J, Zeier WG. A solid future for battery development. *Nat Energy*. 2016; 1: 16141.
2. Varzi A, Raccichini R, Passerini S, Scrosati B. Challenges and prospects of the role of solid electrolytes in the revitalization of lithium metal batteries. *J Mater Chem A*. 2016; 4: 17251-17259.
3. Wu B, Lochala J, Taverne T, Xiao J. The interplay between solid electrolyte interface (SEI) and dendritic lithium growth. *Nano Energy*. 2017; 40: 34-41.
4. Niu C, Liu D, Lochala JA, Anderson CS, Cao X, Gross ME, et al. Balancing interfacial reactions to achieve long cycle life in high-energy lithium metal batteries. *Nat Energy*. 2021; 6: 723-732.
5. Ge Z, Li J, Liu J. High sodium ion mobility of PEO-NaTFSI- $\text{Na}_3\text{Zr}_2\text{Si}_2\text{PO}_{12}$  composite solid electrolyte for all-solid-state Na-S battery. *ChemistrySelect*. 2022; 7: e202200620.
6. Maurya DK, Dhanusuraman R, Guo Z, Angaiah S. Composite polymer electrolytes: Progress, challenges, and future outlook for sodium-ion batteries. *Adv Compos Hybrid Mater*. 2022; 5: 2651-2674.
7. Boschini A, Johansson P. Characterization of NaX (X: TFSI, FSI) - PEO based solid polymer electrolytes for sodium batteries. *Electrochim Acta*. 2015; 175: 124-133.
8. Moreno JS, Armand M, Berman MB, Greenbaum SG, Scrosati B, Panero S. Composite PEO<sub>n</sub>: NaTFSI polymer electrolyte: Preparation, thermal and electrochemical characterization. *J Power Sources*. 2014; 248: 695-702.
9. Singh MD, Dalvi A, Phase DM. Electrical transport in PEO-NaI-NASICON nanocomposites: An assessment using impedance and X-Ray absorption spectroscopy. *Mater Res Bull*. 2019; 118: 110485.
10. Ma Q, Tsai CL, Wei XK, Heggen M, Tietz F, Irvine JT. Room temperature demonstration of a sodium superionic conductor with grain conductivity in excess of  $0.01 \text{ S cm}^{-1}$  and its primary applications in symmetric battery cells. *J Mater Chem A*. 2019; 7: 7766-7776.
11. Matsumoto K, Matsui T, Nohira T, Hagiwara R. Crystal structure of  $\text{Na}[\text{N}(\text{SO}_2\text{CF}_3)_2]$  and coordination environment of alkali metal cation in the  $\text{M}[\text{N}(\text{SO}_2\text{CF}_3)_2]$  ( $\text{M}^+ = \text{Li}^+, \text{Na}^+, \text{K}^+, \text{and Cs}^+$ ) structures. *J Fluor Chem*. 2015; 174: 42-48.
12. Brooks DJ, Merinov BV, Goddard III WA, Kozinsky B, Mailoa J. Atomistic description of ionic diffusion in PEO-LiTFSI: Effect of temperature, molecular weight, and ionic concentration. *Macromolecules*. 2018; 51: 8987-8995.
13. Caruso T, Capoleoni S, Cazzanelli E, Agostino RG, Villano P, Passerini S. Characterization of PEO-lithium triflate polymer electrolytes: Conductivity, DSC and raman investigations. *Ionics*. 2002; 8: 36-43.
14. Choo Y, Halat DM, Villaluenga I, Timachova K, Balsara NP. Diffusion and migration in polymer electrolytes. *Prog Polym Sci*. 2020; 103: 101220.
15. Golodnitsky D, Ardel G, Peled E. Ion-transport phenomena in concentrated PEO-based composite polymer electrolytes. *Solid State Ion*. 2002; 147: 141-155.
16. Jiang Y, Yan X, Ma Z, Mei P, Xiao W, You Q, et al. Development of the PEO based solid polymer electrolytes for all-solid state lithium ion batteries. *Polymers*. 2018; 10: 1237.
17. Yu P, Popov BN, Ritter JA, White RE. Determination of the lithium ion diffusion coefficient in graphite. *J Electrochem Soc*. 1999; 146: 8.

18. Persson K, Sethuraman VA, Hardwick LJ, Hinuma Y, Meng YS, Van Der Ven A, et al. Lithium diffusion in graphitic carbon. *J Phys Chem Lett.* 2010; 1: 1176-1180.
19. Hayamizu K, Seki S. Long-range Li ion diffusion in NASICON-type  $\text{Li}_{1.5}\text{Al}_{0.5}\text{Ge}_{1.5}(\text{PO}_4)_3$  (LAGP) studied by  $^7\text{Li}$  pulsed-gradient spin-echo NMR. *Phys Chem Chem Phys.* 2017; 19: 23483-23491.
20. Wiemers Meyer S, Winter M, Nowak S. NMR as a powerful tool to study lithium ion battery electrolytes. *Annu Rep NMR Spectrosc.* 2019; 97: 121-162.
21. Hayamizu K, Tsuzuki S, Seki S, Umebayashi Y. Nuclear magnetic resonance studies on the rotational and translational motions of ionic liquids composed of 1-ethyl-3-methylimidazolium cation and bis (trifluoromethanesulfonyl) amide and bis (fluorosulfonyl) amide anions and their binary systems including lithium salts. *J Chem Phys.* 2011; 135: 084505.
22. Han KS, Bazak JD, Chen Y, Graham TR, Washton NM, Hu JZ, et al. Pulsed field gradient nuclear magnetic resonance and diffusion analysis in battery research. *Chem Mater.* 2021; 33: 8562-8590.
23. Volkov VI, Chernyak AV, Golubenko DV, Tverskoy VA, Lochin GA, Odjigaeva ES, et al. Hydration and diffusion of  $\text{H}^+$ ,  $\text{Li}^+$ ,  $\text{Na}^+$ ,  $\text{Cs}^+$  ions in cation-exchange membranes based on polyethylene-and sulfonated-grafted polystyrene studied by NMR technique and ionic conductivity Measurements. *Membranes.* 2020; 10: 272.
24. Bilyk SA, Tverskoy VA, Chernyak AV, Avilova IA, Slesarenko NA, Volkov VI. Water molecules' and lithium cations' mobility in sulfonated polystyrene studied by nuclear magnetic resonance. *Membranes.* 2023; 13: 725.
25. Volkov VI, Chernyak AV, Avilova IA, Slesarenko NA, Melnikova DL, Skirda VD. Molecular and ionic diffusion in ion exchange membranes and biological systems (cells and proteins) studied by NMR. *Membranes.* 2021; 11: 385.
26. Volkov VI, Yarmolenko OV, Chernyak AV, Slesarenko NA, Avilova IA, Baymuratova GR, et al. Polymer electrolytes for Lithium-ion batteries studied by NMR techniques. *Membranes.* 2022; 12: 416.
27. Indris S, Heitjans P, Uecker R, Roling B. Li ion dynamics in a  $\text{LiAlO}_2$  single crystal studied by  $^7\text{Li}$  NMR spectroscopy and conductivity measurements. *J Phys Chem C.* 2012; 116: 14243-14247.
28. Kaus M, Guin M, Yavuz M, Knapp M, Tietz F, Guillon O, et al. Fast  $\text{Na}^+$  ion conduction in NASICON-type  $\text{Na}_{3.4}\text{Sc}_2(\text{SiO}_4)_{0.4}(\text{PO}_4)_{2.6}$  observed by  $^{23}\text{Na}$  NMR relaxometry. *J Phys Chem C.* 2017; 121: 1449-1454.
29. Epp V, Ma Q, Hammer EM, Tietz F, Wilkening M. Very fast bulk Li ion diffusivity in crystalline  $\text{Li}_{1.5}\text{Al}_{0.5}\text{Ti}_{1.5}(\text{PO}_4)_3$  as seen using NMR relaxometry. *Phys Chem Chem Phys.* 2015; 17: 32115-32121.
30. Ladenstein L, Lunghammer S, Wang EY, Miara LJ, Wilkening HM, Redhammer GJ, et al. On the dependence of ionic transport on crystal orientation in NASICON-type solid electrolytes. *J Phys Energy.* 2020; 2: 035003.
31. Deng Y, Eames C, Nguyen LH, Pecher O, Griffith KJ, Courty M, et al. Crystal structures, local atomic environments, and ion diffusion mechanisms of scandium-substituted sodium superionic conductor (NASICON) solid electrolytes. *Chem Mater.* 2018; 30: 2618-2630.
32. Griffin JM, Forse AC, Grey CP. Solid-state NMR studies of supercapacitors. *Solid State Nucl Magn Reson.* 2016; 74: 16-35.
33. Blanc F, Leskes M, Grey CP. In situ solid-state NMR spectroscopy of electrochemical cells: Batteries, supercapacitors, and fuel cells. *Acc Chem Res.* 2013; 46: 1952-1963.

34. Kraft MA, Ohno S, Zinkevich T, Koerver R, Culver SP, Fuchs T, et al. Inducing high ionic conductivity in the lithium superionic argyrodites  $\text{Li}_{6+x}\text{P}_{1-x}\text{Ge}_x\text{S}_5\text{I}$  for all-solid-state batteries. *J Am Chem Soc.* 2018; 140: 16330-16339.
35. Wilkening M, Heitjans P. Li jump process in h- $\text{Li}_{0.7}\text{TiS}_2$  studied by two-time  $^7\text{Li}$  spin-alignment echo NMR and comparison with results on two-dimensional diffusion from nuclear magnetic relaxation. *Phys Rev B.* 2008; 77: 024311.
36. Volgmann K, Epp V, Langer J, Stanje B, Heine J, Nakhal S, et al. Solid-state NMR to study translational Li ion dynamics in solids with low-dimensional diffusion pathways. *Z Phys Chem.* 2017; 231: 1215-1241.
37. Epp V, Gün O, Deiseroth HJ, Wilkening M. Highly mobile ions: Low-temperature NMR directly probes extremely fast  $\text{Li}^+$  hopping in argyrodite-type  $\text{Li}_6\text{PS}_5\text{Br}$ . *J Phys Chem Lett.* 2013; 4: 2118-2123.
38. Epp V, Wilkening M. Li-ion dynamics in solids as seen via relaxation NMR. In: *Handbook of Solid State Batteries*. Singapore: World Scientific Publishing Co Pte Ltd; 2016. pp. 133-190.
39. Langer J, Epp V, Heitjans P, Mautner FA, Wilkening M. Lithium motion in the anode material  $\text{LiC}_6$  as seen via time-domain  $^7\text{Li}$  NMR. *Phys Rev B.* 2013; 88: 094304.
40. Epp V, Nakhal S, Lerch M, Wilkening M. Two-dimensional diffusion in  $\text{Li}_{0.7}\text{NbS}_2$  as directly probed by frequency-dependent  $^7\text{Li}$  NMR. *J Phys Condens Matter.* 2013; 25: 195402.
41. Ma Q, Guin M, Naqash S, Tsai CL, Tietz F, Guillon O. Scandium-substituted  $\text{Na}_3\text{Zr}_2(\text{SiO}_4)_2(\text{PO}_4)$  prepared by a solution-assisted solid-state reaction method as sodium-ion conductors. *Chem Mater.* 2016; 28: 4821-4828.
42. Abragam A. *The principles of nuclear magnetism*. Oxford, UK: Oxford university press; 1961.
43. Slichter CP. *Principles of Magnetic Resonance*. Berlin, Germany: Springer Science & Business Media; 1996.
44. Mehring M. *Principles of High Resolution NMR in Solids*. Berlin, Germany: Springer; 1983. p. 327.
45. Mehring M, Kanert O. Line shape analysis of spin echo signals in cubic solids. *Z Naturforsch A.* 1969; 24: 768-774.
46. Mehring M, Kanert O. Effect of lattice disorder on the line shape of NMR spin echo signals. *Z Naturforsch A.* 1969; 24: 332-336.
47. Furó I, Halle B. 2D quadrupolar-echo spectroscopy with coherence selection and optimized pulse angle. *J Magn Reson.* 1992; 98: 388-407.
48. Kunwar AC, Turner GL, Oldfield E. Solid-state spin-echo fourier transform NMR of  $^{39}\text{K}$  and  $^{67}\text{Zn}$  salts at high field. *J Magn Reson.* 1986; 69: 124-127.
49. Storek M, Böhmer R. Quadrupolar transients, cosine correlation functions, and two-dimensional exchange spectra of non-selectively excited spin-3/2 nuclei: A  $^7\text{Li}$  NMR study of the superionic conductor lithium indium phosphate. *J Magn Reson.* 2015; 260: 116-126.
50. Kimmich R. *Field-cycling NMR relaxometry. NMR: Tomography, Diffusometry, Relaxometry*. Berlin, Germany: Springer, Berlin, Heidelberg; 1997.
51. Bloembergen N, Purcell EM, Pound RV. Relaxation effects in nuclear magnetic resonance absorption. *Phys Rev.* 1948; 73: 679.
52. Zimmer G, Mehring M, Goze C, Rachdi F. Rotational dynamics of  $\text{C}^{4-60}$  and electronic excitation in  $\text{Rb}_4\text{C}_{60}$ . *Phys Rev B.* 1995; 52: 13300-13305.

53. Zimmer G, Thier KF, Mehring M, Rachdi F, Fischer JE.  $^{87}\text{Rb}$  NMR and the T' problem in  $\text{Rb}_3\text{C}_{60}$ . Phys Rev B. 1996; 53: 5620-5625.
54. Zimmer G, Mehring M, Rachdi F, Fischer JE. Vortex dynamics in  $\text{Rb}_3\text{C}_{60}$  observed by  $^{87}\text{Rb}$  and  $^{13}\text{C}$  NMR. Phys Rev B. 1996; 54: R3768-R3771.
55. Mehrer H, Fulde P, von Klitzing K. Diffusion in Solids: Fundamentals, Methods, Materials, Diffusion-Controlled Processes. Berlin, Heidelberg, Germany: Springer Berlin Heidelberg; 2009.
56. Wilkening M, Bork D, Indris S, Heitjans P. Diffusion in amorphous  $\text{LiNbO}_3$  studied by  $^7\text{Li}$  NMR-Comparison with the nano-and microcrystalline material. Phys Chem Chem Phys. 2002; 4: 3246-3251.
57. Baklanova YV, Arapova IY, Buzlukov AL, Gerashenko AP, Verkhovskii SV, Mikhalev KN, et al. Localization of vacancies and mobility of lithium ions in  $\text{Li}_2\text{ZrO}_3$  as obtained by  $^{6,7}\text{Li}$  NMR. J Solid State Chem. 2013; 208: 43-49.
58. Zimmer G, Helmle M, Mehring M, Rachdi F. Lattice dynamics and  $^{13}\text{C}$  paramagnetic shift in  $\text{K}_4\text{C}_{60}$ . Europhys Lett. 1994; 27: 543-548.
59. Hendrickson JR, Bray PJ. A phenomenological equation for NMR motional narrowing in solids. J Magn Reson. 1973; 9: 341-357.
60. Waugh JS, Fedin EI. Determination of hindered-rotation barriers in solids. Sov Phys Solid State. 1963; 4: 1633-1636.
61. Naqash S, Ma Q, Tietz F, Guillon O.  $\text{Na}_3\text{Zr}_2(\text{SiO}_4)_2(\text{PO}_4)$  prepared by a solution-assisted solid state reaction. Solid State Ion. 2017; 302: 83-91.
62. Saalwächter K, Spiess HW. Solid-State NMR of Polymers. Polym Sci A Compr Ref. 2012; 2: 185-219.
63. Blumler P, Blumich B. NMR imaging of elastomers: A review. Rubber Chem Technol. 1997; 70: 468-518.
64. Stolwijk NA, Heddier C, Reschke M, Wiencierz M, Bokeloh J, Wilde G. Salt-concentration dependence of the glass transition temperature in PEO-NaI and PEO-LiTFSI polymer electrolytes. Macromolecules. 2013; 46: 8580-8588.